Batch Crystallization of a Photochemical: Modeling, Control, and Filtration

H. B. Matthews and James B. Rawlings
Dept. of Chemical Engineering, University of Wisconsin, Madison, WI 53706

Model identification and control were studied for the seeded batch crystallization of an organic, industrial photochemical. The growth and nucleation kinetics are described by empirical power-law expressions in relative supersaturation, and an additional model describing crystal shape dynamics is proposed. The parameters in the kinetic models are estimated from on-line measurements of solute concentration and transmittance. Parameter uncertainty is assessed, and optimal experimental design techniques are used to construct experiments to diminish uncertainty. Given the identified model, optimal open-loop temperature schedules are designed to improve the filtration of final-time slurries. The profiles minimize the mass of nucleated crystal relative to seed crystal mass, subject to supersaturation and yield constraints. Filtration improvements are verified using constant pressure filtration tests to determine the flow resistance of the filter cake. The best control experiment gives a cake resistance 25% lower than the best identification experiment.

Introduction

This article explores the improvement of slurry filtration through the determination of optimal temperature schedules for seeded, batch cooling crystallizers. The temperature schedules are optimized subject to a fundamental model of the dynamics of the crystal-size distribution (CSD). The model is identified for a batch crystallization of an organic photochemical produced currently by the Eastman Kodak Company in its production facilities in Rochester, NY. (The name and chemical formula of the photochemical are protected by a nondisclosure agreement.) The photochemical system is chosen because it is an economically important crystallization that exhibits some of the critical problems associated with industrial crystallizations, including slow growth rates, an irregular crystal habit, a size distribution that is difficult to characterize, and poor filtration.

Model-based optimization of temperature schedules in seeded batch crystallization has been examined by several researchers (Miller and Rawlings, 1994; Ajinkya and Ray, 1974; Mullin and Nývlt, 1971). The benefits of implementing such control policies have been shown to include increased seed crystal size (Mullin and Nývlt, 1971) and increased weight-mean crystal size (Miller and Rawlings, 1994). The optimized objectives (such as weight-mean size) were chosen to serve as scalar metrics accounting for the effect of CSD on filtration rate. However, despite this desire to speed the filtration process via changes in CSD, the explicit evaluation of slurry filtration was not examined in previous model-based control studies. The present study focuses directly on the improvement of filtration properties for final-time crystallization slurries. Slurry filtration is evaluated by determining the average specific flow resistance in the filter cake from constant pressure filtration experiments (Tiller and Crump, 1977).

Correspondence concerning this article should be addressed to J. B. Rawlings.

Experimental Apparatus

The experimental apparatus used in this study is similar to that described by Miller and Rawlings (1994). The crystallizer is a 3-L, glass, jacketed batch vessel. The temperature of the crystallizer is controlled precisely by a model predictive controller that manipulates the water temperature in the jacket. The controller design allows precise trajectory tracking during the identification and optimal control experiments presented in this article.

Three types of on-line measurements are recorded during the crystallization experiments. Slurry temperature data are provided by an *in-situ* resistance temperature detector (RTD) at intervals of 15 s. A transmittance measurement is provided

by an *in-situ* colorimeter probe. This probe is situated in the crystallizer headplate and extends downward into the slurry. The incident light from the colorimeter source is projected through a stream of flowing slurry (perpendicular to the flow), to a mirror and then back to the colorimeter sensor. The total beam length is 2 mm. The measurement is recorded at 2-min intervals. Solution phase concentration of the solute is measured with a densitometer. This measurement requires an external, solids-free stream that is recycled to the crystallizer. The measurement is recorded at 20-s intervals.

Additional elements of the experimental apparatus include data acquisition and control hardware and a workstation that performs on-line control calculations and stores the collected data. The photochemical is crystallized from heptane. The apparatus is described in greater detail by Miller (1993) and Matthews (1997).

Model Formulation

The population balance model used to describe the batch crystallizer apparatus is similar to that presented by Miller and Rawlings (1994). The CSD of the slurry is modeled by a deterministic population balance equation. The PBE model is a partial differential equation in time and crystal size L.

$$\frac{\partial f(L,t)}{\partial t} = -G\frac{\partial f(L,t)}{\partial L}. \tag{1}$$

where $f(L,t)$ is the CSD and G is the size-independent crystal growth rate. In the present study the characteristic size is taken to be crystal width.

The solution phase concentration in the crystallizer is described by a mass balance on the crystallizing solute

$$\frac{d\hat{C}}{dt} = -3\rho_c k_v h G \int_0^\infty f(L,t)L^2 dL \tag{2}$$

where $\hat{C}$ is the concentration in mass of solute per mass solvent (mass solute/mass solvent), ρ_c is the crystal density, k_v is the volume shape factor converting L^3 into crystal volume and h converts solvent mass to slurry volume.

The initial forms of the kinetic expressions are taken to be empirical power-laws in relative supersaturation

$$G = k_g S^g \tag{3}$$

$$B^0 = k_b S^b \mu_3^j \tag{4}$$

where S is relative supersaturation, B^0 is the nucleation rate at zero size, μ_3 is the third moment of the CSD. The parameters k_g, g, k_b, b, and j were inferred from experimental data.

The Beer-Lambert law is used to relate the transmittance measurement to the second moment of the CSD

$$\frac{I}{I_0} = \exp\left[-\frac{lk_a}{2}\int_0^\infty f(L,t)L^2 dL\right] \tag{5}$$

I is the intensity of the light transmitted through the slurry, I_0 is the intensity of the incident light, l is the beam length, and k_a is the area shape factor.

The solution of Eqs. 1 and 2 requires appropriate boundary and initial conditions. The zero-size boundary condition of Eq. 1 is defined as

$$f(0,t) = \frac{B^0}{G|_{L=0}}. \tag{6}$$

The initial conditions for the population and mass balances, respectively, are

$$f(L,t) = f_s(L), \qquad t = 0 \tag{7a}$$

$$\hat{C}(t) = \hat{C}_0, \qquad t = 0 \tag{7b}$$

where $f_s(L)$ is the size distribution of the seeds. Because the CSD of the seed crystals may not be determined explicitly, $f_s(L)$ is assumed to be a linear decay from zero size to a maximum seed size, L_m. The linear distribution has the form

$$f_s(L) = f_l\left(1 - \frac{L}{L_m}\right), \qquad 0 \le L \le L_m \tag{8}$$

where f_l is the population density at zero size. L_m is determined from scanning electron and optical micrographs and the zero-size intercept is determined by a mass balance on the seeds. A detailed treatment of the seed side distribution is given by Matthews (1997). The PBE of Eq. 1 is solved using the method of moments. Miller (1993) provides a complete description of the batch crystallizer model.

Inference of Model Parameters from Data

Probability theory provides a unifying approach for parameter estimation problems. Given the data Y and the model, the goal is to find the posterior density function of the model parameters θ. The optimal parameter estimates are those that locate the maximum, or mode, of the probability density function.

Consider the following assumptions about the prediction errors:

- The prediction errors are normally distributed with zero mean and covariance matrix V.
- Prediction errors corresponding to different sample times are uncorrelated.
- Prediction errors corresponding to the m different measurement types are uncorrelated.
- The prediction errors are homoscedastic (error variance is independent of the magnitude of the measured variable).

Under these assumptions, the model parameters that select the maximum of the Bayesian posterior density function also minimize the objective function

$$\Phi_{be} = \sum_{k=1}^{m} (n_k + 1)\ln\left[\sum_{i=1}^{n_k} e_{ik}^2(\boldsymbol{\theta})\right]. \tag{9}$$

where n_k is the number of measurements of the kth type and e_{ik} is the prediction error of the ith measurement of the kth type. Given the optimal model parameters $\hat{\theta}$ the maximum-density estimate of the prediction variance for the kth measurement type $\hat{\sigma}_k^2$, is

$$\hat{\sigma}_k^2 = \frac{\sum_{i=1}^{n_k} e_{ik}^2(\hat{\boldsymbol{\theta}})}{n_k + 1} \tag{10}$$

An approximation of the spread of the posterior density may be obtained by assuming that the model can be represented as linear in the parameters in the vicinity of the modal estimates. Linearization allows the determination of the Gaussian Hessian $\boldsymbol{H}_{\theta\theta}$ which describes the curvature of the distribution about the mode.

Marginal confidence intervals for the model parameters may be determined according to

$$\theta_i \approx \hat{\theta}_i \pm \sqrt{\chi_p^2(\alpha)\boldsymbol{H}_{\theta\theta}^{-1}(i,i)} \tag{11}$$

where $\boldsymbol{H}_{\theta\theta}^{-1}(i,i)$ is i, i element of $H_{\theta\theta}^{-1}$. The linear 95% confidence intervals cited throughout the remainder of this article were calculated according to Eq. 11 with $\alpha = 0.025$.

More detailed presentations of Bayesian inference of parameters from data are given by Stewart et al. (1992), Box and Tiao (1973) and Matthews (1997).

Initial Estimation of Kinetic Parameters

The kinetic parameters given in Eqs. 3 and 4 were estimated from experimental data collected for the photochemical-heptane system. The parameter vector of the initial model has the form

$$\boldsymbol{\theta} = \begin{bmatrix} kg & : & \text{growth rate constant} \\ g & : & \text{growth rate order} \\ k_b & : & \text{nucleation rate constant} \\ b & : & \text{nucleation rate order} \\ j & : & \text{nucleation crystal mass order} \end{bmatrix} \tag{12}$$

The parameters were estimated by posing a nonlinear program (NLP) with the Bayesian objective function of Eq. 9. The method may be summarized in the following statement of the unconstrained NLP.

$$\begin{array}{ll} \min_{\boldsymbol{\theta}} & \Phi_{be}\left[Y, \tilde{Y}(\boldsymbol{\theta}); \hat{\boldsymbol{\sigma}}\right] \\ \text{subject to:} & \text{crystallizer model:} \end{array} \tag{NLP1}$$

The sequential quadratic programming code NPSOL (Gill et al., 1986) was used to solve this unconstrained optimization problem.

The designs of the identification experiments were differentiated by initial seed mass and temperature profile. In most experiments, the seed crystals were introduced at high levels of supersaturation. This method was used to maximize the dynamic information in the data for experiment durations of six to ten hours. The seeding policy also provided a margin of safety to prevent the dissolution of the small seed loads. This policy protected against the possibility of errors in the estimated solubility curve or the bulk temperature measurement. The seeds were not classified by size because replicable mechanical separation was not practical given the small size and needle-like habit of the crystals. The seed masses were small to allow the collection of meaningful transmittance data, but were varied for different experiments. The temperature schedules used in the identification experiments are given in Figure 1. In each experiment, the seeds were added at time = 0. Figure 1 shows the actual crystallizer temperature data. The set point trajectories are not shown, because they would be obscured by the data. The set point tracking is more than adequate for the purposes of this study.

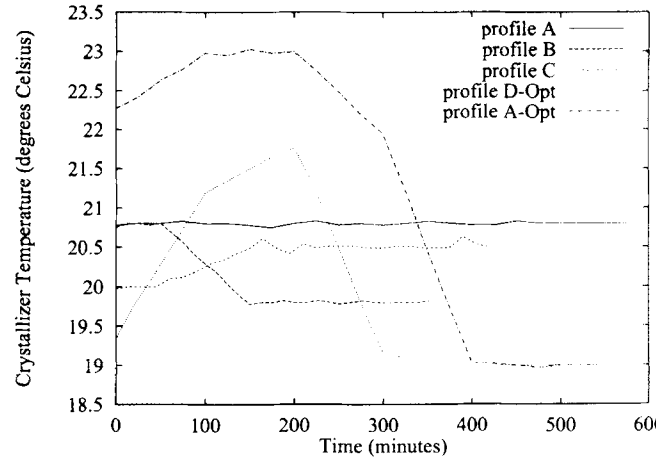

Figure 1. Representative temperature schedules from identification batch crystallization experiments.

The D-Opt and A-Opt temperature schedules in Figure 1 are optimal experimental designs constructed to minimize the uncertainty in the parameter estimates. The optimal designs were determined by posing a nonlinear program to identify piecewise linear temperature profiles minimizing either the determinant of $H_{\theta\theta}^{-1}$ or the normalized trace of $H_{\theta\theta}^{-1}$. The former objective is termed D-Optimal design and was first suggested for nonlinear models by Box and Lucas (1959). The A-Optimal normalized trace objective was proposed by Pinto et al. (1991). A detailed discussion of these optimal experimental designs is given by Matthews (1997).

The temperature schedules and seed loads for the 11 experiments are summarized in Table 1. The initial concentration was 0.11 g photochemical/g heptane for each experiment.

The optimal kinetic parameters are determined given the data from the 11 runs described in Table 1. The resulting transmittance and concentration residuals for runs 3a, 3b, 4a and 4b are given in Figures 2 and 3. Clearly, the transmittance data are not well-described by the initial model. The parameter estimates are not given because the large transmittance residuals of Figure 2 suggest that they are not meaningful. It is not possible to determine parameters for the standard power-law models of Eq. 3 and 4 that describe simultaneously the transmittance and concentration data. Thus, revisions in the model are required.

Table 1. Seed Loads and Cooling Profiles for the Identification Experiments

Run No.	Seed Mass (g)	Cooling Policy
1c	0.0517	profile A
2a	0.1023	profile B
2b	0.0983	profile B
2c	0.1004	profile B
3a	0.1489	profile C
3b	0.1527	profile C
4a	0.0740	profile C
4b	0.0745	profile C
4c	0.0731	profile C
5a	0.1496	profile D-Opt
A-Opt	0.2501	profile A-Opt

Model Extensions: Dynamic Shape and Size-Dependent Nucleation

Two extensions are made to allow the model to describe the crystallization data. A single parameter model is proposed to describe changes in the crystal habit of the seeds and the secondary nucleation model is extended to account for the sizes of the colliding crystals. Both revisions are required to attain adequate predictions of the data.

Dynamic shape model

Neglecting breakage, crystal habit is determined by the relative growth rates of the individual faces of a crystal (Mullin, 1993). These growth rates are commensurate with the ease in which new solute molecules are incorporated into the crystal lattice structure of a particular face. If one face grows quickly relative to others, the crystal dimension perpendicular to that face grows as well, resulting in larger facial areas for slower growing faces.

The original model assumed a constant parallelepiped shape that was determined from scanning electron micrographs of the seeds. However, the micrographs also indicated that many of the seed crystals were broken. If, due to breakage from filtration or milling, the initial habit was different from the growth derived habit, the crystal shape of the seeds may have changed during the experiments. Such habit dynamics would prevent the transmittance and concentration

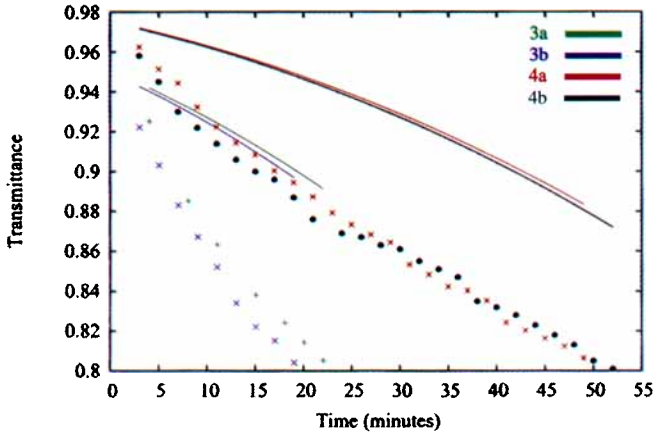

Figure 2. Transmittance residuals for runs 3a, 3b, 4a and 4b.

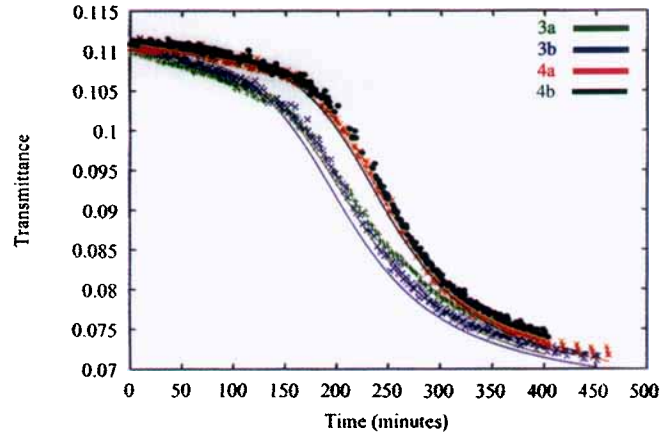

Figure 3. Concentration residuals for runs 3a, 3b, 4a and 4b.

models from providing consistent predictions due to inappropriate volume and area shape factors (see k_v and k_a in Eqs. 2 and 5, respectively).

Breakage is assumed to diminish the length of the seed crystals, but not the depth or width. This assumption allows shape dynamics to be modeled as changes in length-to-width ratio l_w. Given a seed with initial width $L(0)$ a dynamic model of l_w for an individual crystal is

$$l_w(t) = \frac{l_w(0)L(0) + l_w(\infty)\Delta L(t)}{L(0) + \Delta L(t)} \tag{13}$$

where $l_w(0)$ is the initial length-to-width ratio determined from SEM or optical micrographs, $\Delta L(t) = \int_0^t G dt$, and $l_w(\infty)$ is the asymptotic length-to-width ratio as ΔL goes to infinity. The parameter $l_w(\infty)$ is an estimate of the ratio of the growth rates along the length and width dimensions. For parallelepiped crystals, the area and volume shape factors may be expressed as

$$k_a = 2(l_w d_w + l_w + d_w) \tag{14}$$

$$k_v = l_w d_w \tag{15}$$

where d_w is the depth-to-width ratio.

Equation 13 depends on $L(0)$. This dependence, illustrated in Figure 4, may be integrated out by averaging Eq. 13 over the initial size distribution of the seeds. For the linear seed distribution of Eq. 8, the dynamic average is

$$\overline{l_w}(t) = l_w(0) + \frac{2\Delta L}{L_m}[l_w(0) - l_w(\infty)] \times \left[1 + \left(1 + \frac{\Delta L}{L_m}\right)\ln\left(\frac{\Delta L}{L_m + \Delta L}\right)\right] \tag{16}$$

The $\overline{l_w}(t)$ profile corresponding to Eq. 16 with $L_m = 20$ micron is also presented in Figure 4.

The habit change model is implemented by computing ΔL with the other states of the extended model. Given an initial estimate of $l_w(0)$, the instantaneous value of ΔL and the pa-

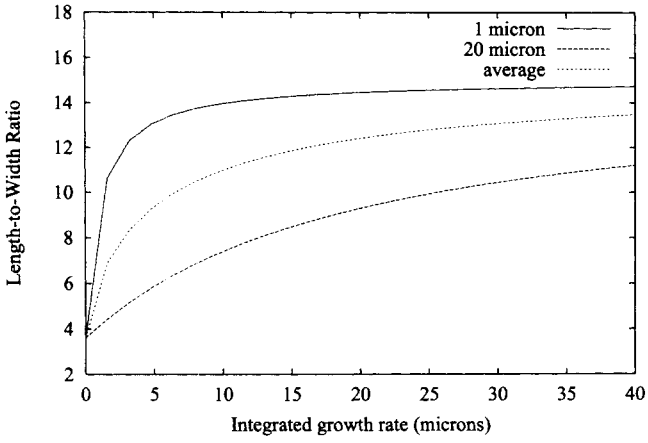

Figure 4. Dependence of length-to-width ratios on integrated growth rate.

Evolution for a linear distribution averaged ratio is contrasted with profiles for individual crystals of 1 and 20 micron widths. The asymptotic limit as integrated growth rate goes to infinity is 15.

rameter $l_w(\infty)$ allows subsequent determination of $l_w(t)$, $k_a(t)$ and $k_v(t)$. The habit dynamics are only applied to the seed crystals. The nuclei are assumed to have the habit dictated by $l_w(\infty)$. The parameter $l_w(\infty)$ is estimated from the data.

Size-dependent nucleation

The size-dependent nucleation model is a variation of that proposed by Ottens et al. (1972). The model has the form

$$B^0 = k_b S^b \mu_3 (L_{\min})^j \tag{17}$$

where $L_{\min}$ is the minimum size required for a crystal to participate in collisions that produce secondary nuclei. The critical value of $L_{\min}$ accounts for the fact that smaller crystals are less likely to produce nuclei, because they have lower collisional probabilities and energies (small area, small mass, adherence to fluid streamlines). Rousseau et al. (1976) and Kubota and Fujiwara (1990) provide empirical support for the minimum size assumption in the magnesium sulfate and potassium alum chemical systems, respectively. The studies of Rousseau et al. and Kubota and Fujiwara (1990) each show $L_{\min} \approx 200\ \mu$m. $L_{\min}$ is also estimated from the data.

Estimation of Parameters for the Extended Model

The extended crystallizer model incorporates the dynamic habit and size-dependent nucleation submodels. The revised parameter vector contains seven parameters

Table 2. Parameter Estimates and 95% Confidence Intervals for the Optimal Extended Model Using All Available Concentration, Transmittance, and Optical Microscope Data

	$\ln(k_g)$	g	$\ln(k_b)$	b	j	$L_{\min}$	$l_w(\infty)$
Estimate	−1.39	1.76	26.94	2.91	2.20	27.08	11.18
Interval	±0.04	±0.02	±0.57	±0.18	±0.08	±0.67	±0.81

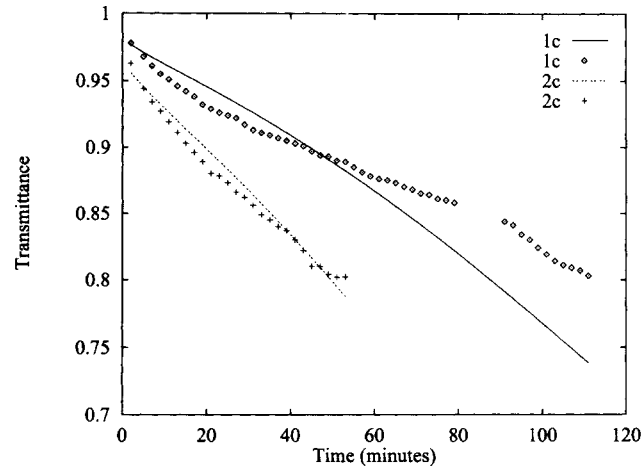

Figure 5. Transmittance profiles and model fits for runs 1c and 2c using the parameters in Table 2.

$$\theta = \begin{bmatrix} k_g & : & \text{growth rate constant} \\ g & : & \text{growth rate order} \\ k_b & : & \text{nucleation rate constant} \\ b & : & \text{nucleation rate order} \\ j & : & \text{nucleation crystal mass order} \\ L_{\min} & : & \text{minimum crystal size for nucleation} \\ l_w(\infty) & : & \text{asymptotic length-to-width ratio} \end{bmatrix} \tag{18}$$

The model parameters were estimated using transmittance and concentration data from the 11 crystallization experiments. The modal parameter estimates and their 95% linear confidence intervals are given in Table 2. The data sets and model predictions are given in Figures 5 through 10. The improved fit of the transmittance data given by the extended model is clear.

The 95% confidence intervals in Table 2 indicate that the optimal parameter estimates are precisely identified. The op-

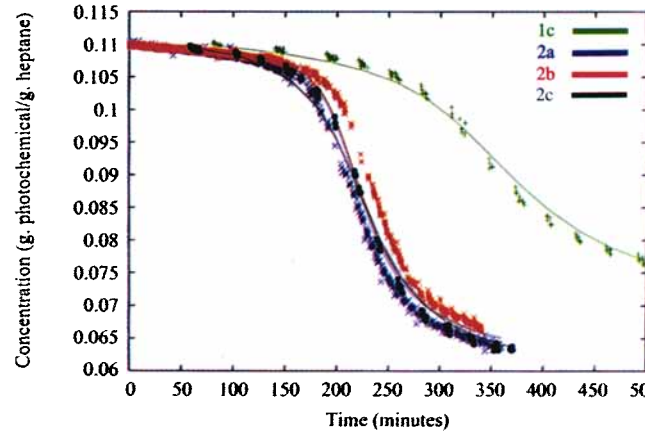

Figure 6. Concentration profiles and model fits for runs 1c, 2a, 2b and 2c using the parameters in Table 2.

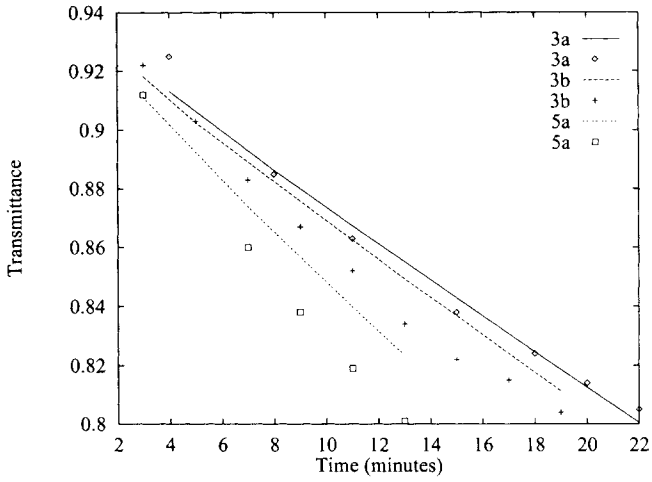

Figure 7. Transmittance profiles and model fits for runs 3a, 3b and 5a using the parameters in Table 2.

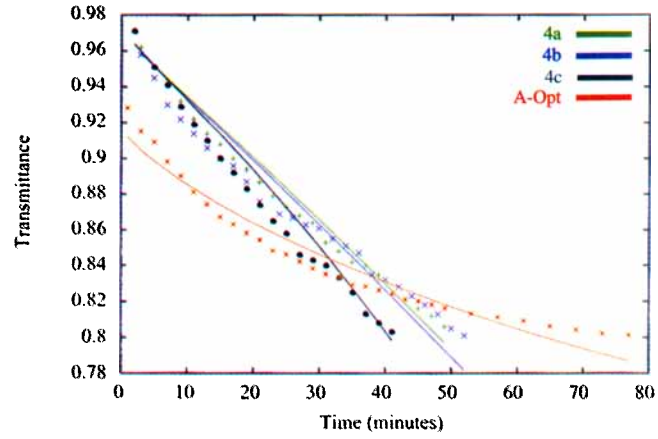

Figure 9. Transmittance profiles and model fits for the A-Optimal design and runs 4a, 4b and 4c using the parameters in Table 2.

timal estimates of b and q indicate that the nucleation process is higher order in relative supersaturation than is growth. Higher-order nucleation suggests that low driving force levels suppress nucleation relative to growth. The third moment order of nucleation j is 2.20 indicating that crystal-crystal collisions are more influential than crystal-agitator contacts in creating nuclei. When crystal-agitator contacts dominate, j is usually found to be closer to one than to two. Values near two are rare, but have been observed in lab-scale crystallizers (van der Heijden et al., 1994).

The crystal shape dynamics described by Eq. 16 and the optimal value of $l_w(\infty)$ were confirmed via optical microscopy. At five times during the A-Optimal experiment, 1 mL slurry samples were drawn from the crystallizer and examined using an optical microscope. Representative photographs of the sampled crystals are given in Figures 11 and 12. Figure 12 depicts crystals that have undergone a width coordinate size increase of approximately 8 μm. There is a clear increase in the length-to-width ratios of the crystals from the time of initial seeding.

Length-to-width ratios for 96 crystals in the five slurry samples were measured from the photographs and included in the data set used to estimate the optimal parameters of Table 2. The fit of the model to the length-to-width ratio data is given in Figure 13. Despite the noise in the data, the dynamic shape model clearly allows the extended model to account for shape changes.

Optimal Control to Improve Filtration

Miller and Rawlings (1994) developed an optimization-based method for determining optimal temperature schedules for batch crystallizers. The method determined the temperature profiles by minimizing an objective function subject to absolute bounds on temperature and constraints on cooling rate, supersaturation range, and final-time yield. The present study applies the optimal control method of Miller and Rawlings to determine a temperature profile minimizing the final-time mass of nucleated crystals relative to the mass of grown seed crystals (m_N/m_S). The idea of relating filtration rate to the fraction of nucleated crystal mass in a batch crystallizer was introduced by Jones et al. (1987). Miller and Rawlings determined m_N/m_S-optimal profiles for the KNO_3-

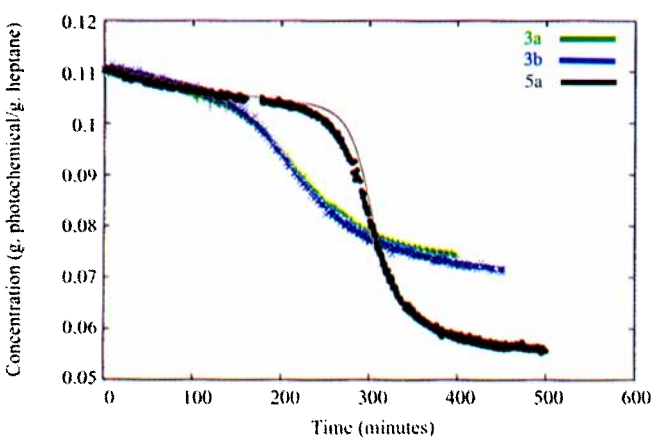

Figure 8. Concentration profiles and model fits for runs 3a, 3b and 5a using the parameters in Table 2.

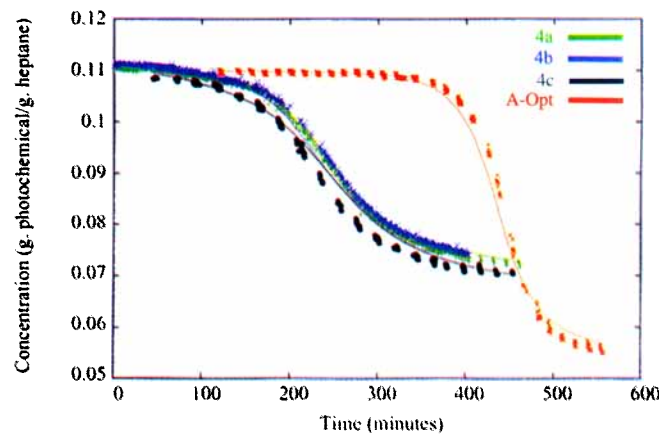

Figure 10. Concentration profiles and model fits for the A-Optimal design and runs 4a , 4b and 4c using the parameters in Table 2.

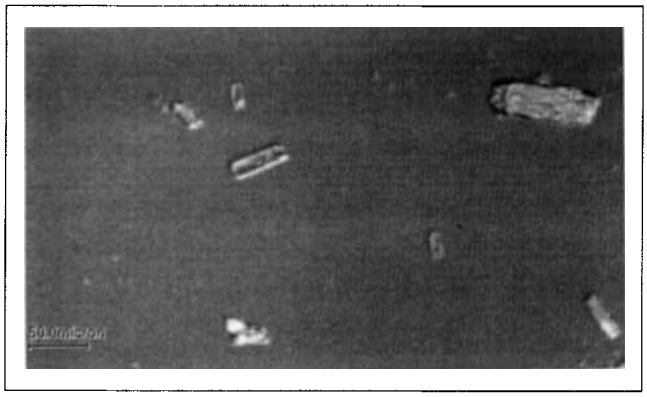

Figure 11. Optical micrograph of low length-to-width ratio seed crystals.

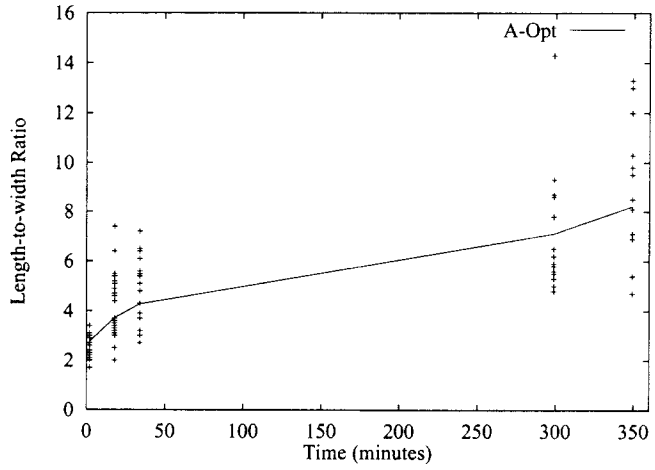

Figure 13. Length-to-width ratio vs. time profile for the A-Optimal experiment.

H_2O system but the filtration characteristics of optimized policies were not evaluated.

The optimal temperature schedules applied in this study were determined for a temperature range between 18.5 and 24.0°C. The profile duration was 550 min with the vertices defining the piecewise-linear temperature profile placed at 55 min intervals. This discretization gave a decision variable vector T with 11 elements. Maximum and minimum constraints on relative supersaturation were set to 1.0 and 0, respectively. The optimal policy was constrained to provide a minimum solute yield of 50%.

The optimal temperature profile and corresponding relative supersaturation profile are given in Figure 14. The form of the optimal temperature profile may be explained in terms of the effect of the relative supersaturation profile on the kinetic processes of crystal nucleation and growth. The low seed load (0.25 g) limits nucleation at the beginning of the experiment; therefore, the driving force may be very high to increase seed size without producing nuclei. As the mass of large crystals in the system increases, nucleation occurs at progressively higher rates. Since nucleation is higher order in supersaturation than is growth (see Table 2), the relative supersaturation is reduced to a low plateau for most of the experiment in order to favor growth. At the end of the experiment, the driving force increases slightly to meet the yield constraint. This late increase does produce nuclei, but the run is discontinued before they can attain appreciable mass.

A parametric analysis of the optimal profile shows that increases in seed mass and profile duration improve the predicted final-time value of m_N/m_S and that the policy is robust to the uncertainty in the kinetic parameters (Matthews, 1997).

Filtration Testing

Constant pressure filtration tests were performed for two m_N/m_S-optimal control experiments and for 9 of the 11 model identification experiments. The filterability measure used to quantify the quality of a filtration is the average specific resistance to fluid flow within a filter cake. As shown by Tiller and Crump (1997), for a constant pressure filtration the average specific cake resistance $\bar{\alpha}_c$ may be determined from the linear relationship given below

$$\frac{t}{m_f} = \frac{\bar{\alpha}_c \nu_f c_f}{2A_f^2 P} m_f + \frac{R_m \nu_f}{A_f P}. \tag{19}$$

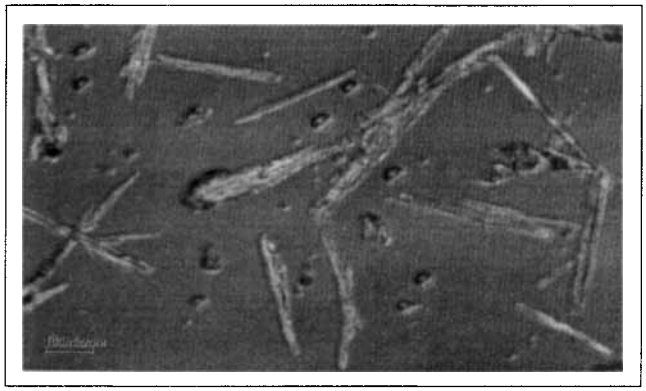

Figure 12. Optical micrograph of high length-to-width ratio crystals later in same crystallization.

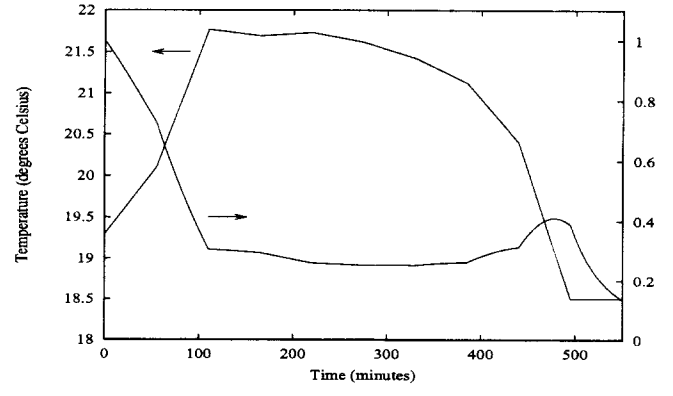

Figure 14. Simulated temperature and relative supersaturation profiles minimizing m_N/m_S using the optimal model of Table 2.

where t is filtration time, m_f is filtrate mass, ν_f is the kinematic viscosity of the filtrate, c_f is the mass of dry crystal per unit mass of filtrate, A_f is the filtration area, P the applied pressure and R_m the flow resistance of the filter medium. The filtration tests were conducted at a constant pressure of 5.5 psig (37.9 kPa).

Two profiles optimizing the m_N/m_S objective function were implemented for the photochemical-heptane system. These profiles were optimized for seed mass of 0.25 and 0.15 grams, respectively, to demonstrate the effect of seed load on filtration performance. Due to a change in the photochemical raw material stock, the fits of the optimal model to the measured concentration profiles of the optimized runs was reasonable but not as good as the fits shown for the identification experiments. The change in the system kinetics due to a change in the raw material stock suggests that there is significant batch-to-batch variation in the photochemical system. A detailed description of the control profile implementation is given by Matthews (1997).

Table 3 presents a summary of the cake resistance values determined for both the identification experiments and the control experiments. Where replicates are available (that is, runs 2, 3 and 4), the values in Table 3 are averages. Replicate experiments exhibited $\overline{\alpha}_c$ variations of about 15%. This variation emphasizes that filtration measurements tend to be noisy and difficult to replicate.

Table 3 shows that the lowest cake resistance values recorded in this study corresponded to the two optimal profiles. The $\phi_{0.25}$ (0.25-g seed mass) experiment had a cake resistance 25% lower than any of the identification experiments in the study. Also, despite having higher solids densities, the optimized slurries filtered faster than those from all but one of the previous experiments. These points confirm that the optimization of m_N/m_S does improve the filtration qualities of the resulting slurries. Further evidence is provided by plotting $\overline{\alpha}_c$ vs. the $m_N(t_f)/m_S(t_f)$ objective function for each of the filtered slurries. This plot is given in Figure 15.

The data in Figure 15 suggest a correlation between $m_N(t_f)/m_S(t_f)$ and cake resistance. This correlation may be summarized by calculating the linear correlation coefficient. The correlation coefficient for $\overline{\alpha_c}$ vs. the predicted value of $m_N(t_f)/m_S(t_f)$ is given in Table 4. Table 4 also presents correlation coefficients describing relationships between $\overline{\alpha_c}$ and predicted final-time values of the weight-mean coefficient of variation (c_{vw}) and the weight-mean size ($\overline{L_w}$). The values in Table 4 suggest that the optimization strategies minimizing the final-time values of m_N/m_S and c_{vw} or maximizing the final-time value of $\overline{L_w}$ may provide improvements in the flow resistance of crystallized filter cakes.

Table 3. Summary of Constant Pressure Filtration Tests

Run Type	No. Samples	$\overline{\alpha_c}$ (cm/g)	% Solids	Time (s)
1	1	1.97×10^9	5.8	54.0
2	2	2.51×10^9	7.3	99.0
3	2	1.66×10^9	5.8	62.0
4	2	2.72×10^9	5.8	75.1
5	1	2.56×10^9	8.4	81.4
A-Opt	1	2.49×10^9	8.7	92.9
$^*\phi_{0.15}$	1	1.44×10^9	8.9	58.7
$^*\phi_{0.25}$	1	1.14×10^9	8.9	51.8

$^*\phi_{0.15}$ and $\phi_{0.25}$ designate optimized temperature schedules for seed loads of 0.15 and 0.25 g, respectively.

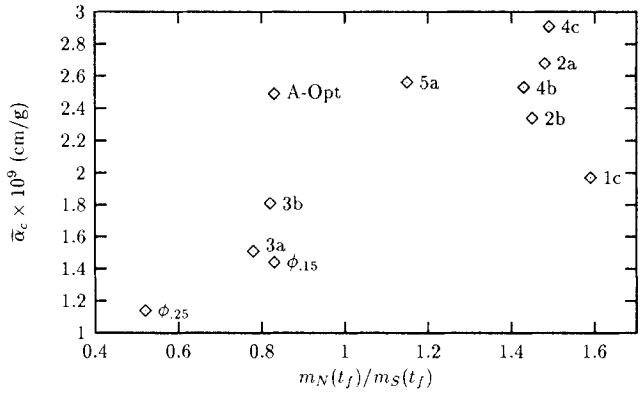

Figure 15. Correlation between average specific cake resistance and predicted values of $m_N(t_f)/m_S(t_f)$.

$\phi_{0.15}$ and $\phi_{0.25}$ refer to experiments optimized for seed loads of 0.15 and 0.25 g, respectively.

Conclusions

This article has described the successful application of a fundamental modeling approach to describe the evolution of the CSD for the seeded batch crystallization of a photochemical from a heptane solvent. The photochemical described is currently produced by the Eastman Kodak Company. Empirical models of crystal nucleation and growth were identified and a novel model for describing dynamic changes in crystal shape was proposed, identified, and confirmed. The parameters in the kinetic models were estimated by minimizing a Bayesian objective function and parameter uncertainty was evaluated. Optimal experimental design techniques were employed to design experiments to reduce parameter uncertainty. There are, of course, alternative models, such as growth rate dispersion models, that might explain the data (Zumstein and Rousseau, 1987). Given the data in this study, the application of statistical techniques to discriminate between such rival models would be an interesting topic for future research.

Given the identified model, an optimization of the open-loop temperature profile was conducted to attempt to improve the filtration of the final-time crystallization slurries. An optimal temperature profile minimizing the mass of nucleated crystals relative to the mass of seed crystals (m_N/m_S) was determined. The form of the optimal profile was described in terms of the kinetic expressions and parameters.

Two optimal control experiments, utilizing different seed loads, were implemented. Constant pressure filtration tests on the final-time slurries indicated that the flow resistance of the filter cake was lowered for the two optimized experi-

Table 4. Correlation Coefficients Describing the Linear Relationships between $\overline{\alpha}_c$ and Predicted Final-time Values of m_N/m_S, c_{vw}, and $\overline{L}_w$

	m_N/m_S	c_{vw}	$\overline{L}_w$
Correlation Coefficient	0.73	0.84	−0.91

ments relative to the experiments used to identify the model. The slurries produced by the optimal control experiments filtered faster than previous slurries despite having higher solids densities, and the optimal experiment utilizing the higher seed load had a cake resistance 25% lower than that of the best identification experiment. Comparisons of cake resistance values for experiments with identical temperature schedules but different seed loads indicated that higher seed loads improved filtration. Lastly, correlation coefficients were determined for cake resistance vs. predicted final-time values of m_N/m_S, weight-mean coefficient of variation, and weight-mean size. These correlations indicated that lower flow resistance in the filter cake was correlated with low values of m_N/m_S and weight-mean coefficient of variation and high values of weight-mean size.

Acknowledgments

Financial support from Eastman Kodak Company, the National Science Foundation under grant CTS-8957123, and the International Fine Particle Research Institute is gratefully acknowledged.

Notation

$\hat{C}_o$ = initial solution phase concentration (mass solute/mass solvent)
$\overline{l_w}(t)$ = seed distribution averaged crystal length-to-width ratio
m = number of measurement types
m_N = mass of nucleated crystals
m_S = mass of seed crystals
p = number of model parameters
t_f = final time of an experiment
T = slurry temperature
$\bar{Y}$ = matrix of model predictions
α = confidence level of χ_p^2
ΔL = integral of crystal growth rate
μ_i = ith moment of the CSD
σ = vector of measurement standard deviations
$\hat{\sigma}$ = vector of modal measurement standard deviations
ρ_f = filtrate density
Φ_{be} = Bayesian objective function
χ_p^2 = Chi-squared distribution with p degrees of freedom

Literature Cited

Ajinkya, M. B., and W. H. Ray, "On the Optimal Operation of Crystallization Processes," *Chem. Eng. Commun.*, **1**, 181 (1974).

Box, G. E. B., and H. L. Lucas, "Design of Experiments in Non-linear Situations," *Biometrika*, **46**, 77 (1959).

Box, G. E. P., and G. C. Tiao, *Bayesian Inference in Statistical Analysis*, 1st ed., Addison-Wesley Publishing, Reading, MA (1973).

Gill, P. E., W. Murray, M. A. Saunders, and M. H. Wright, "User's Guide for SOL/NPSOL (Version 4.0): A Fortran Package for Nonlinear Programming," Technical Report SOL 86-2, Systems Optimization Lab., Dept. of Operations Research, Stanford Univ. (1986).

Jones, A. G., J. Budz, and J. W. Mullin, "Batch Crystallization and Solid-Liquid Separation of Potassium Sulphate," *Chem. Eng. Sci.*, **42**(4), 619 (1987).

Kubota, N., and M. Fujiwara, "Minimum Seed Crystal Size for Secondary Nucleation of Potassium Alun in a Stirred-Vessel Crystallizer," *J. Chem. Eng. Japan*, **23**(6), 691 (1990).

Matthews, H. B., "Model Identification and Control of Batch Crystallization for an Industrial Chemical System," PhD Thesis, Univ. of Wisconsin-Madison (1997).

Miller, S. M., "Modelling and Quality Control Strategies for Batch Cooling Crystallizers," PhD Thesis, The Univ. of Texas at Austin (1993).

Miller, S. M., and J. B. Rawlings, "Model Identification and Control Strategies for Batch Cooling Crystallizers," *AIChE J.*, **40**(8), 1312 (1994).

Mullin, J. W., *Crystallization*, 3rd ed., Butterworth, London (1993).

Mullin, J. W., and J. Nývlt, "Programmed Cooling of Batch Crystallizers," *Chem. Eng. Sci.*, **26**, 369 (1971).

Ottens, E. P. K., A. H. Janse, and E. J. D. Jong, "Secondary Nucleation in a Stirred Vessel Cooling Crystallizer," *J. Cryst. Growth*, **13/14**, 500 (1972).

Pinto, J. C., M. W. Lobão, and J. L. Monteiro, "Sequential Experimental Design for Parameter Estimation: Analysis of Relative Deviations," *Chem. Eng. Sci.*, **46**(12), 3129 (1991).

Rousseau, R. W., K. K. Li, and W. L. McCabe, "The Influence of Seed Crystal Size on Nucleation Rates," *AIChE Symp. Ser.*, **72**(153), 48 (1976).

Stewart, W. E., M. Caracotsios, and J. P. Sørensen, "Parameter Estimation from Multiresponse Data," *AIChE J.*, **38**(5), 641 (1992).

Tiller, F. M., and J. R. Crump, "Solid-Liquid Separation: An Overview," *Chem. Eng. Prog.*, **73**, 65 (1977).

van der Heijden, A. E. D. M., J. P. van der Eerden, and G. M. van Rosmalen, "The Secondary Nucleation Rate: A Physical Model," *Chem. Eng. Sci.*, **49**(18), 3103 (1994).

Zumstein, R. C., and R. W. Rousseau, "Growth Rate Dispersion by Initial Growth Rate Distributions and Growth Rate Fluctuations," *AIChE J.*, **33**(1), 121 (1987).

Manuscript received May 9, 1997, and revision received Jan. 29, 1998.